Supplementary Information (SI) for Journal of Materials Chemistry A.
This journal is © The Royal Society of Chemistry 2024

Supplementary Information

Elucidating the Mechanism of Solid-State Energy Release from Dianthracenes *via* Auto-Catalyzed Cycloreversion

Cijil Raju,[1,‡] Zhenhuan Sun,[1,‡] Ryo Koibuchi,[2,‡] Ji Yong Choi,[3] Subhayan Chakraborty,[1] Jihye Park,[3] Hirohiko Houjou,[2,*] Klaus Schmidt-Rohr,[1,*] and Grace G. D. Han[1,*]

[1]Department of Chemistry, Brandeis University, 415 South Street, Waltham, MA 02453, USA

[2]Institute of Industrial Science, University of Tokyo, 4-6-1 Komaba, Meguro-ku, Tokyo 153-8505, Japan

[3]Department of Chemistry, University of Colorado Boulder, 215 UCB, Boulder, CO 80309, USA

E-mail: gracehan@brandeis.edu, srohr@brandeis.edu, houjou@iis.u-tokyo.ac.jp

[‡]Equal contribution

Table of Contents

1. General Methods

All reagents and starting materials were purchased from commercial suppliers and used as received unless otherwise indicated. Compounds **1**-A, **2**-A and **3**-A were synthesized and dimerized to **1**-D, **2**-D and **3**-D respectively by following the procedure reported previously.[1] The dimerization of anthracenes to dianthracenes was performed by dispersing freshly prepared anthracenes **1**-A and **2**-A in ethanol (100 mg in 10 mL) and **3**-A in diethyl ether (100 mg in 5 mL) and subsequently irradiating the suspensions with 405 nm LED light for 4 h under constant stirring. The dianthracene formation is visually evident from the yellow to white color change of the suspension. The formed crystalline dianthracenes were filtered and washed with the respective solvents used for the suspension. The chemical identification and purity of the dianthracenes were confirmed by solid-state NMR analyses. The solid dianthracenes are stable over 1-6 days at room temperature as per the previous report.[1] Solution-state ^{1}H and ^{13}C NMR spectra were recorded on a Bruker Avance 400 spectrometer at 400 MHz and 100 MHz, respectively. LED lamps for the photochemical reactions were purchased from Thorlabs, Inc., including the models M365L3 (365 nm,14.4 $\mu W/mm^2$, 1290 mW); M405L4 (405 nm, 14.53 $\mu W/mm^2$, 1300 mW).

2. Differential Scanning Calorimetry (DSC)

DSC analyses of all the three samples were recorded on a DSC 250 (TA Instruments) with an RSC 90 cooling component. The temperature dependent DSC analysis of samples was recorded at a heating rate of 10 ℃/min unless otherwise noted. Time dependent (isothermal) DSC analysis of samples was recorded at a constant temperature of 48 °C with an initial preheating delay of 2 minutes from 25 °C to reach 48 °C. Approximately 1-2 mg of each dianthracene was used for all the DSC experiments.

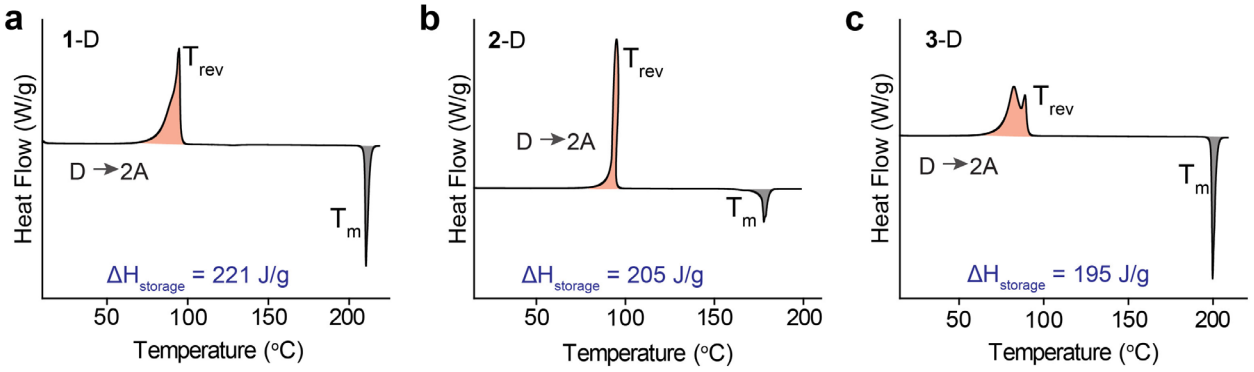

Figure S1. DSC thermograms of a) **1**-D, b) **2**-D, and c) **3**-D respectively indicating cycloreversion of dianthracenes followed by melting of anthracenes. T_{rev}: peak temperature of thermal reversion, T_m: melting point of anthracene

3. Powder X-ray Diffraction (PXRD)

All the time-dependent PXRD analyses were performed using a Rigaku MiniFlex600 diffractometer with a CuKα source (λ= 1.5405 Å) attached with an Anton Paar BTS 150 heating module. The operation and preliminary data analysis was executed using the software SmartLab Studio II. An experimental protocol (step size, 0.020°; speed, 10 °/min; scan duration, 5 min; sample quantity, 20-30 mg) was developed for the time-dependent PXRD analyses of all the dianthracene cycloreversion process. PXRD patterns of all the dianthracene samples were recorded at 25 °C, followed by heating to 49 ± 1 °C. Sample was scanned after 10 minutes of wait time to obtain the isothermal PXRD data after 10 minutes at 49 ± 1 °C. In the subsequent scans the wait time was reduced to 5 minutes to compensate for the scan duration of 5 minutes in the total wait time to 10 minutes. Dianthracenes **1**-D and **2**-D scanned for 360 minutes and **3**-D for 180 minutes. All the samples were scanned after cooling the temperature of BTS 150 to 25 °C.

4. Solid-State NMR

Solid-state NMR experiments were performed on a Bruker Neo Avance 400WB spectrometer at resonance frequencies of 400 MHz for ^{1}H and 100 MHz for ^{13}C, using a 4-mm magic-angle spinning (MAS) double resonance probe head. Each sample, of a mass of 50 to 60 mg, was packed into a 4-mm outer-diameter zirconia rotor with a 3-mm tall cylindrical glass spacer at the bottom and a Kel-F cap at the top. The π/2-pulse durations were 3.6 μs for ^{1}H and 4 μs for ^{13}C. Proton decoupling was conducted with TPPM at $|\gamma B_1|/2\pi = 95$ kHz before detection and with SPINAL-64[2] at $|\gamma B_1|/2\pi = 85$ kHz during detection. Most experiments were performed at 14 kHz MAS, with a rotation-synchronized Hahn echo prior to detection to prevent baseline distortions due to pulse dead-time. One series of experiments at 3 kHz MAS utilized four-pulse total suppression of sidebands (TOSS)[3] instead of the Hahn echo. The ^{13}C chemical shifts were externally referenced to the ^{13}COO resonance of *α*-glycine at 176.49 ppm. All ^{13}C NMR spectra were acquired using ^{1}H-^{13}C composite pulse multiple cross polarization (multiCP) with 5 blocks of 1.1 ms of ramped CP separated by 5 s of repolarization time for a more quantitative transfer of ^{1}H magnetization to ^{13}C. At 14 kHz MAS, the sample temperature was 49 ± 1 ºC due to friction heating and the 3-kHz MAS experiments were performed to study compound **3** at a temperature of ~25 ºC.

Temperature elevation caused by friction heating of 14 kHz MAS was measured through the temperature dependent chemical shift of ^{79}Br of ~15 mg of KBr dispersed in ~45 mg of an aromatic-rich small molecule powder that mimics the environment of anthracene. The sample was first spun up to 3 kHz MAS, with minimal friction heating, and the KBr chemical shift was set to 0 ppm. Then, as soon as the spinning frequency was set to 14 kHz and acceleration ensued, acquisition (with direct ^{79}Br polarization using a recycle delay of ~1 s) was started with 5 s per averaged spectrum in the beginning, then increased to 10 s and at last to 25 s per averaged spectrum at longer times. The chemical shift was observed to quickly elevate and plateau at ~0.7 ppm or ~324 K within ~70 s. The chemical shift was converted to temperature using the linear relation published by Thurber et al.[4]

In the time-dependent kinetic series, moderately short recycle delays of 30 s for the OCH_3 and OAc derivatives (**2** and **3**, respectively) and 10 s for the CH_3 derivative **1** were implemented instead of the usual $4 \times T_{1H}$, which would have been too time-consuming due to the long ^1H spin-lattice relaxation time of these crystalline samples. In order to provide for adequate time resolution of the cycloconversion, each spectrum at 14-kHz MAS was signal averaged for ~0.5 h and each spectrum at 3-kHz MAS for ~1 h. Total experiment times varied depending on the cycloreversion rate of each sample. Reversion completed within 10 h for the CH_3 and OCH_3 derivatives (compounds **1** and **2**, respectively) and within 4 h for the OAc derivative under 14 kHz MAS. At 3 kHz MAS, conversion of the OAc derivative was followed for 120 h.

5. Solid-State ^{13}C Spectra of Monomers and Dimers

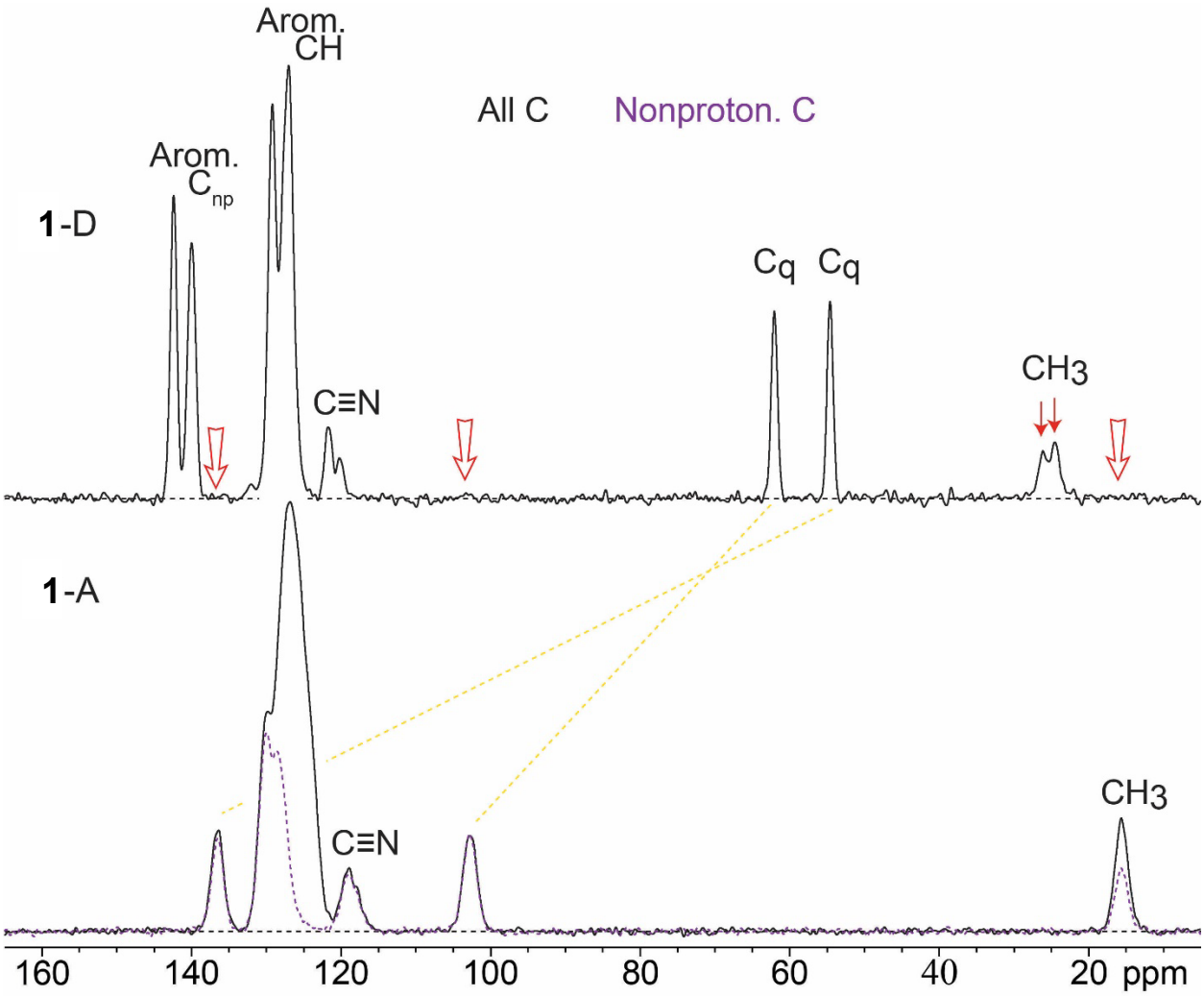

Figure S2. Solid state ^{13}C NMR spectra of **1**-A and **1**-D. Dashed: spectrum after dipolar dephasing. The arrows indicate the disappearance of monomer peaks upon irradiation.

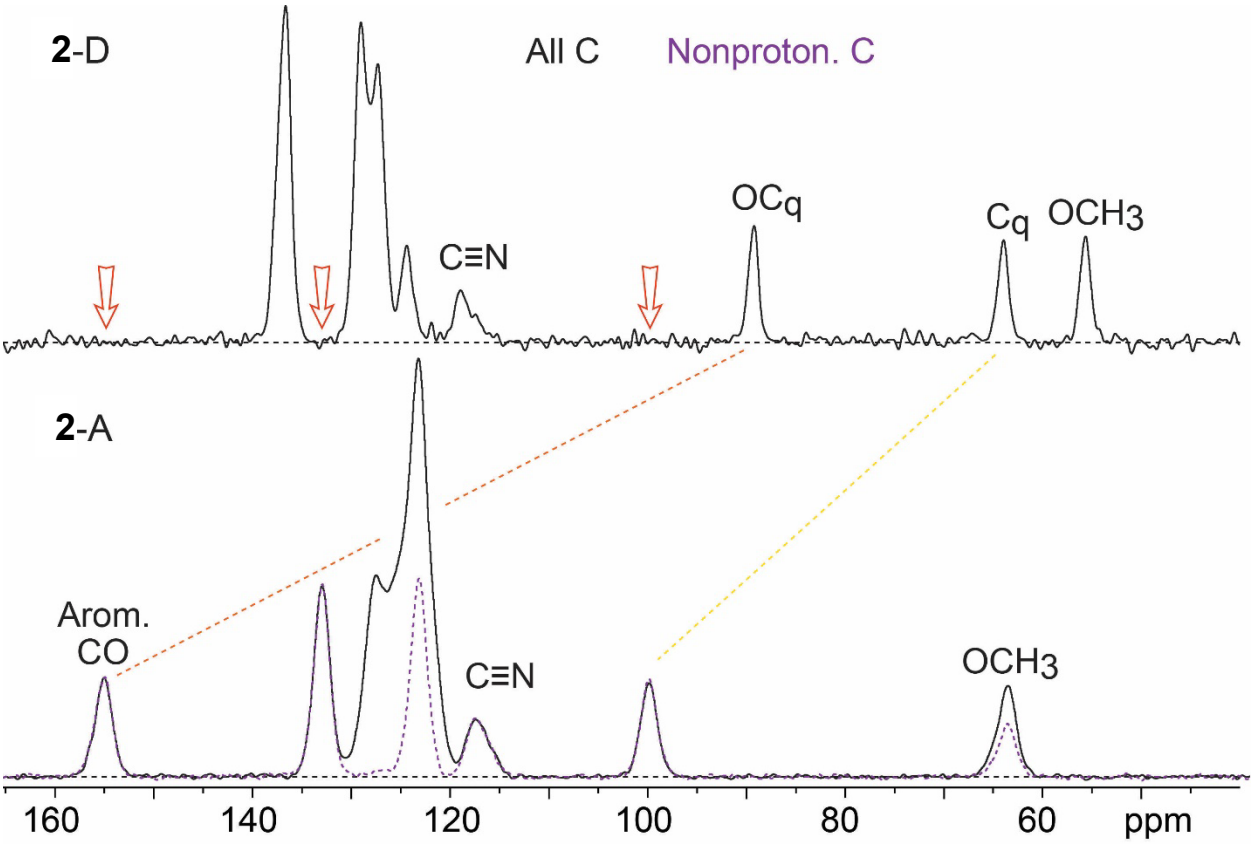

Figure S3. Solid state ^{13}C NMR spectra of **2**-A and **2**-D. Dashed: spectrum after dipolar dephasing. The arrows indicate the disappearance of monomer peaks upon irradiation.

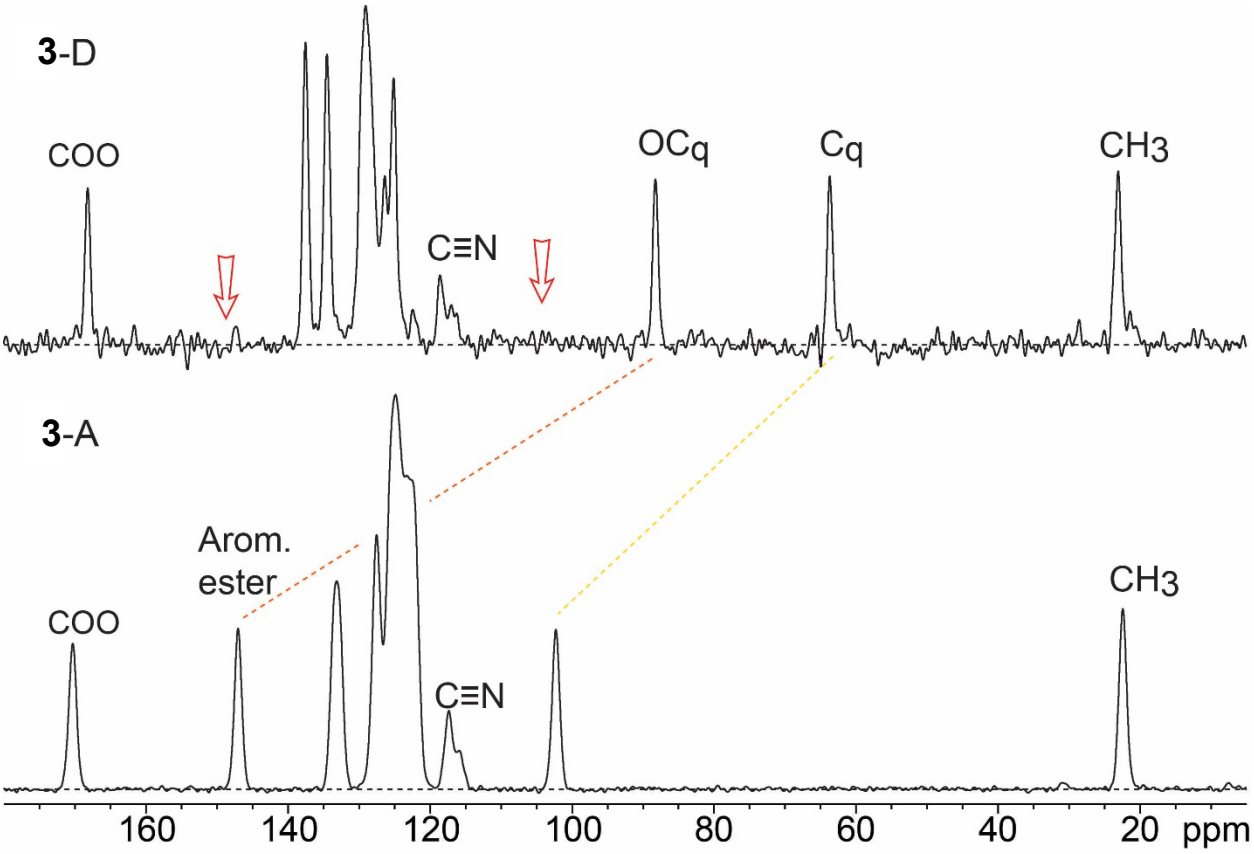

Figure S4. Solid state ^{13}C NMR spectra of **3**-A and **3**-D. The arrows indicate the disappearance of monomer peaks upon irradiation.

6. Solution-State ^{1}H Spectra of Monomers and Dimers

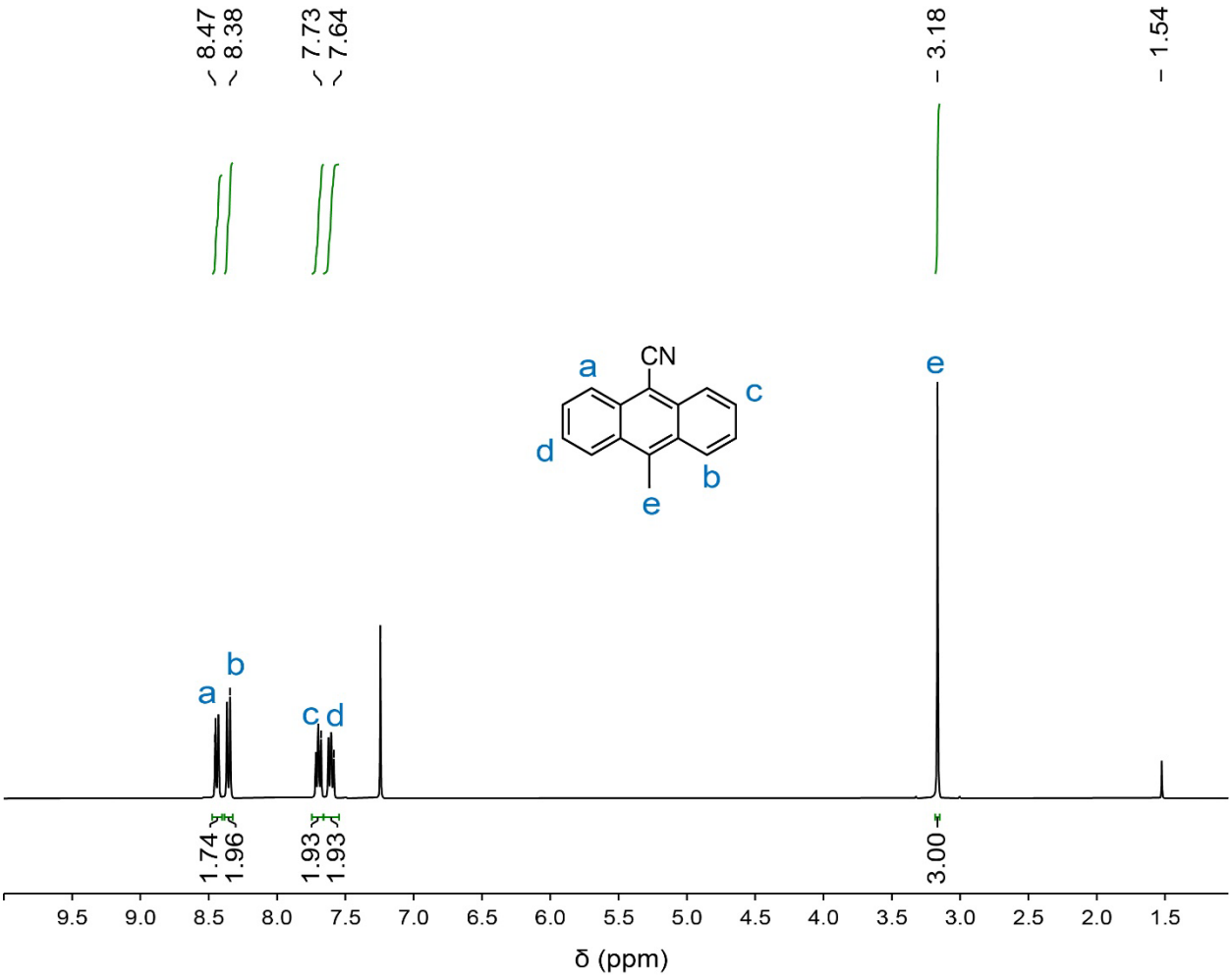

Figure S5. ^{1}H NMR spectrum of **1**-A.

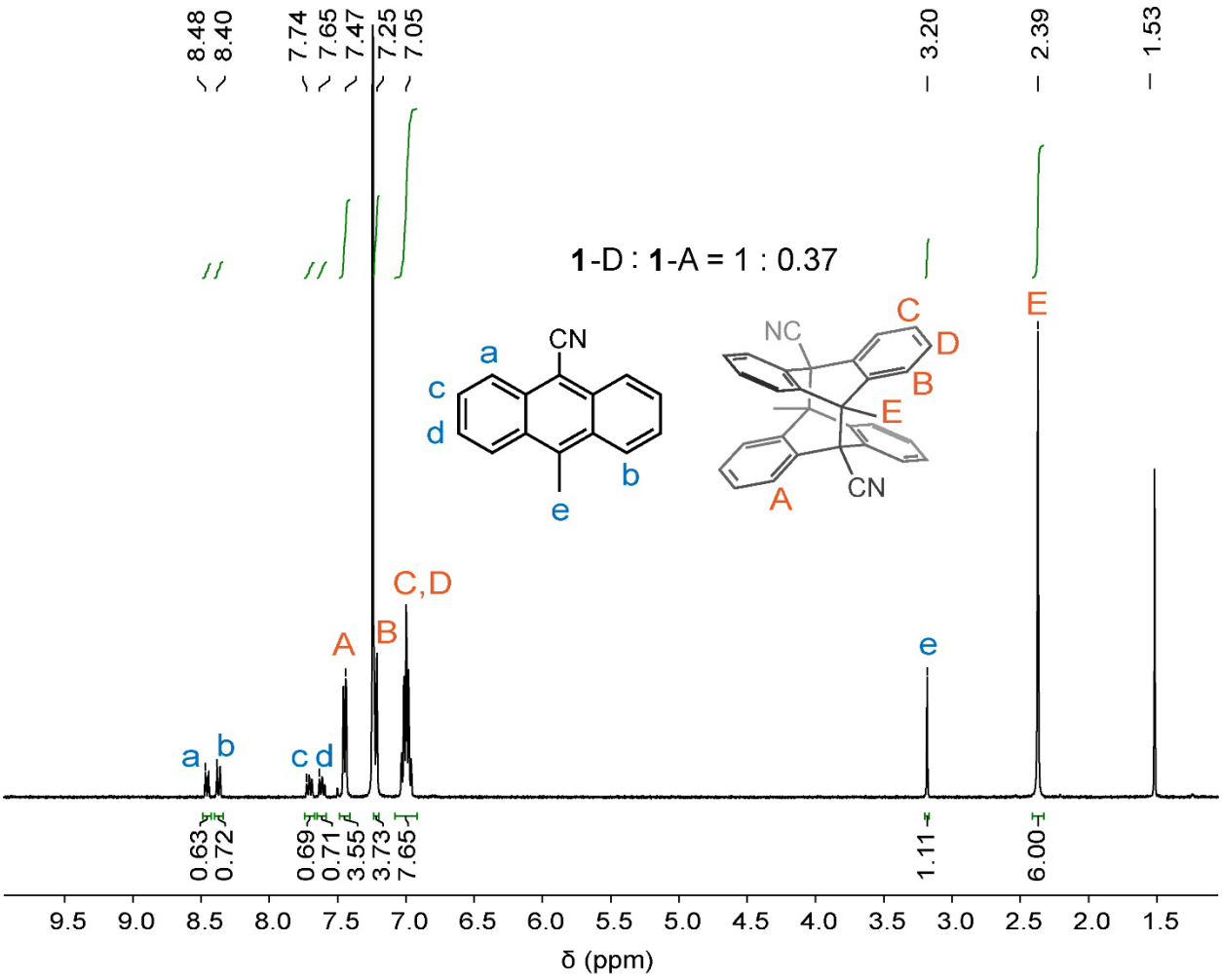

Figure S6. ^{1}H NMR spectrum of **1**-D. The ratio of **1**-D : **1**-A was observed as 1 : 0.37 in $CDCl_3$ due to reversion in solution.

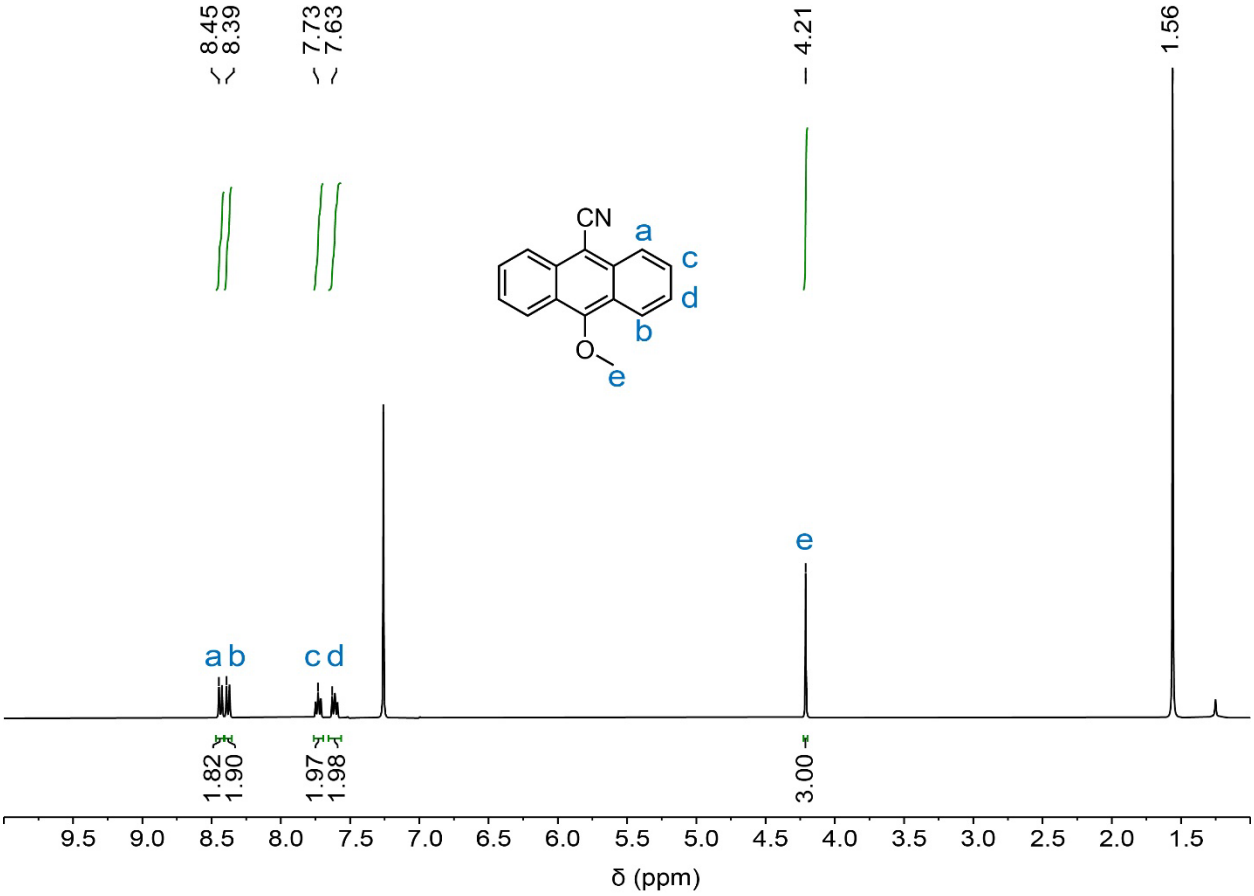

Figure S7. ^{1}H NMR spectrum of **2**-A.

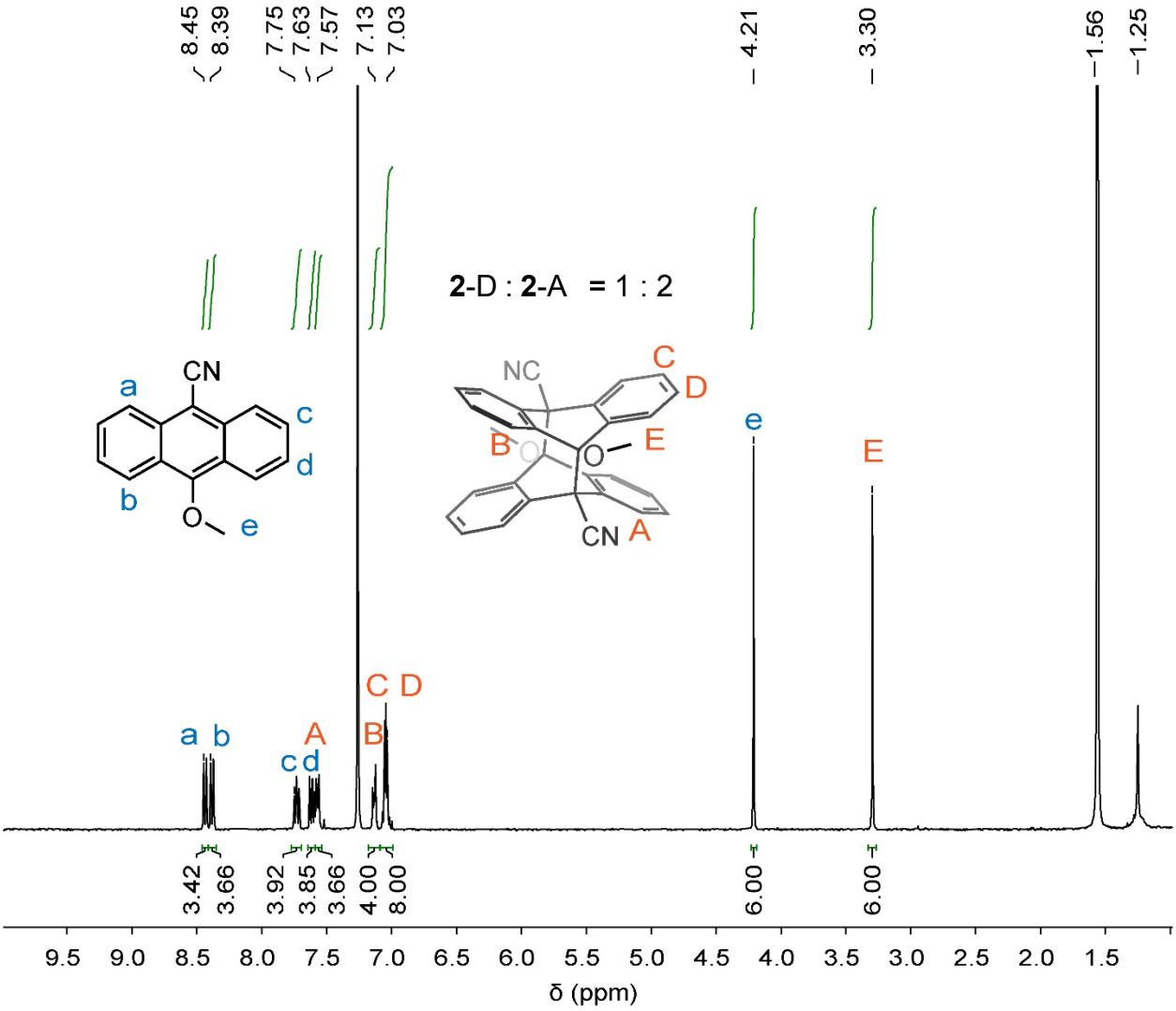

Figure S8. ^{1}H NMR spectrum of **2**-D. The ratio of **2**-D : **2**-A was observed as 1 : 2 in $CDCl_3$ due to reversion in solution.

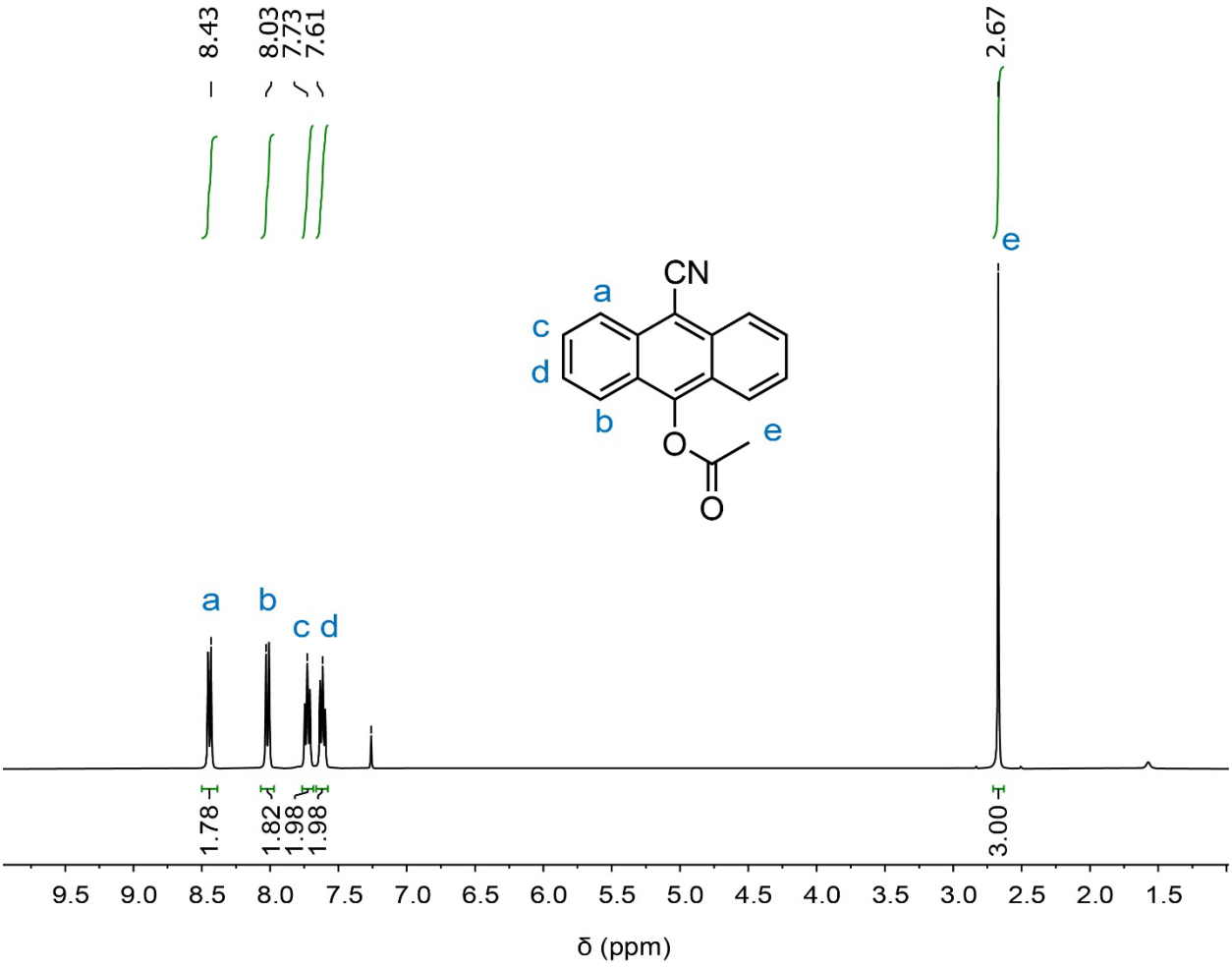

Figure S9. ^{1}H NMR spectrum of **3**-A.

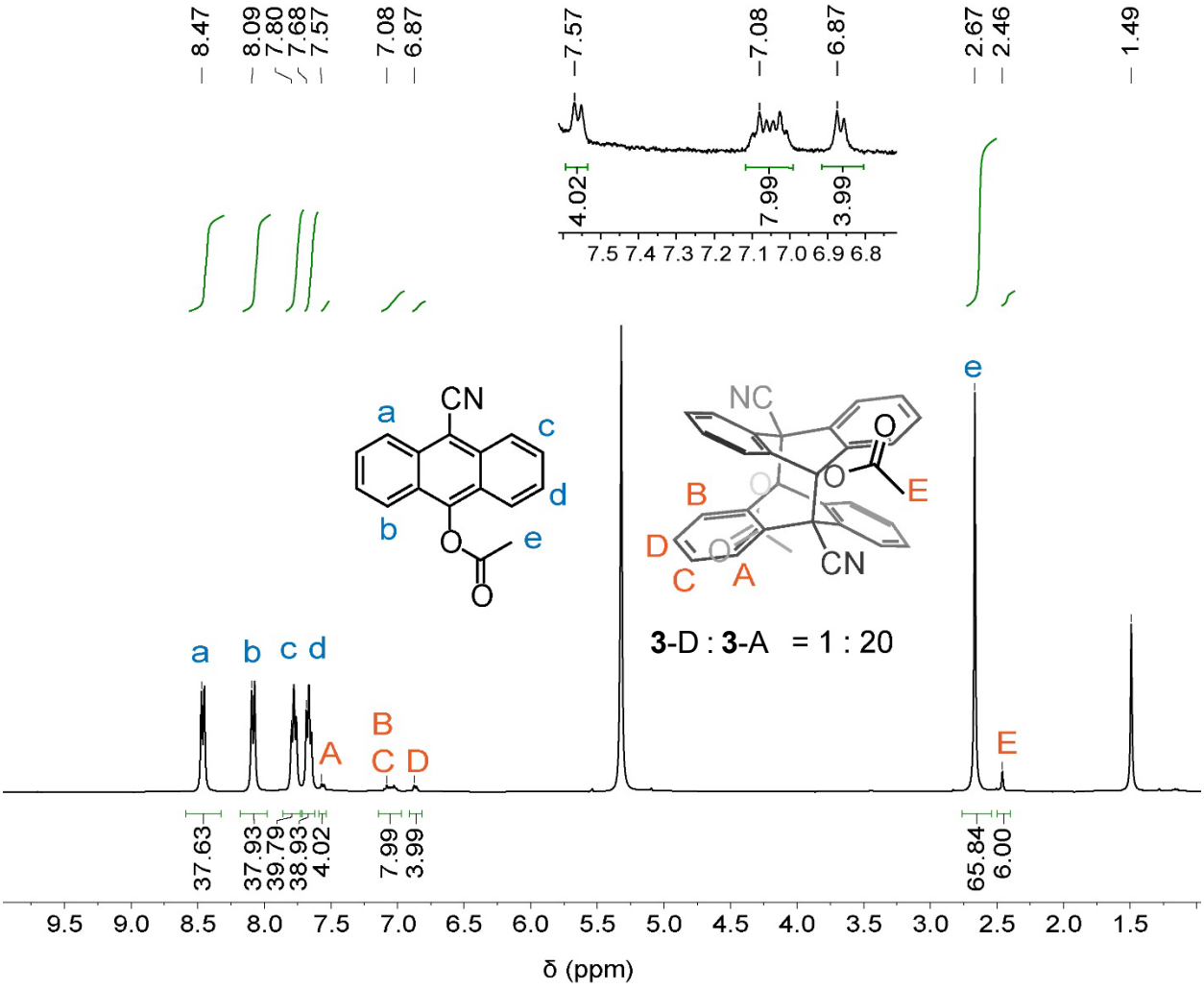

Figure S10. ^{1}H NMR spectrum of **3**-D. The ratio of **3**-D : **3**-A was observed as 1 : 20 in DCM due to reversion in solution.

7. Simulation and Fitting of Cycloreversion Process

Microscopically detailed simulations of cycloreversion were performed on a 32 × 32 × 32 three-dimensional lattice in space using a corresponding matrix in MATLAB. Each matrix entry represented one of three components at that lattice point: a dianthracene, a pair of intermediate anthracenes, or a pair of final crystallized anthracenes. Starting with all dimers, at each timestep the reversion probability was calculated for each dianthracene entry depending on a base probability multiplied by the sum of two cooperativity factors: one based on whether there existed at least one neighbor that has reverted to anthracenes, and the other based on the number of reverted neighbors. A random number was then generated and if the reversion probability was greater than the random number, the dianthracene was converted to an intermediate anthracene pair. After the reversion calculations, potential crystallization of intermediate anthracenes to form the final anthracene crystal was calculated through generation of boxes of size 5 × 5 × 5 (3 × 3 × 3 for the CH_3 derivative **1**) centered at random coordinates. If the fraction of anthracene pairs within each box was above a threshold of 90%, 73% and 96% for compound **1**, **2**, and **3**, respectively, all intermediate anthracene pairs within the box were converted to final-crystal anthracene pairs. The total volume of all boxes sampled at each timestep was at least twice the total volume of the lattice box to guarantee proper coverage comparable to rigorous but much slower systematic moving-frame scanning. A total of 200 timesteps were simulated and fractions of the three components were determined at each timestep. All simulations were repeated 32 times and averaged to suppress numerical noise.

The resulting curves were compared with the series of experimental datapoints from NMR and fitting parameters (base probability, two cooperative factors and the crystallization threshold) were adjusted to obtain good fits. It needs to be noted that these fitting parameters are not unique; for instance, the OCH_3 dianthracene decay curve can be fitted with (base probability, first cooperativity factor, second cooperativity factor) values of (5×10^{-6}, 6500, 150), (5×10^{-5}, 300, 35) and (5×10^{-4}, 13, 4), where the individual values vary by orders of magnitude but the overall maximum probability is similar around ~0.05. This behavior is unsurprising: our simulation scheme can be considered to resemble the Avrami model [Five JMAK papers] that describes simultaneous nucleation (with rate $\dot{n}$, corresponding to our base probability) and cooperative growth (with speed v, akin to our cooperativity factors). Avrami processes with the same $\dot{n}v^3$ are known to have the same Avrami parameter K and therefore the same conversion behavior.

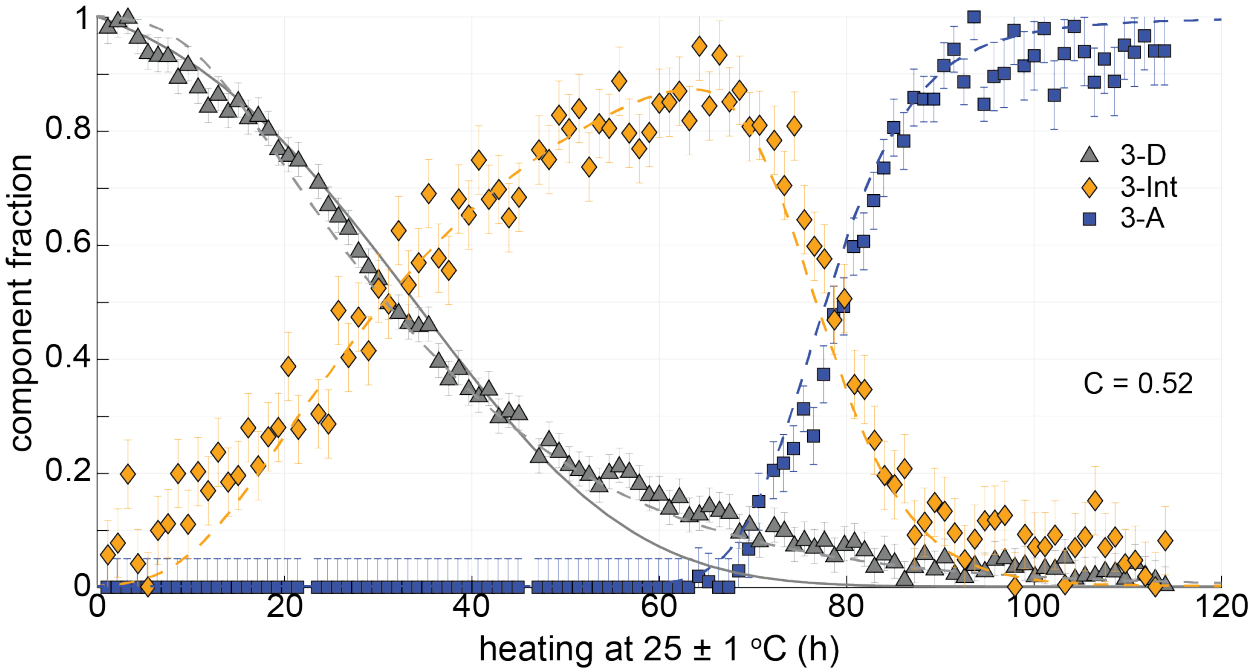

Figure S11. Time dependence, from isothermal solid-state NMR, of the fractions of dianthracene (grey triangles), intermediate anthracene in dianthracene crystals (orange diamonds), and final anthracene crystals (blue squares) during the cycloreversion of **3**-D to **3**-A at 25 °C. The dashed fit curves were obtained from microscopically detailed models as described in the main text. The solid curve has been obtained from a modification of Avrami theory with partial cooperativity, and a cooperativity parameter (*C*) has been derived from it.

8. Computational Methods

For the calculation using QE, the Perdew-Burke-Ernzerhof (PBE) exchange correlational functional was employed to solve the Kohn-Sham equations under the periodic boundary conditions.[5] The dispersion force effect was incorporated by the semiempirical Grimme's D3BJ dispersion correction scheme.[6] The convergence threshold for self-consistency was set to 10^{-8}. For the atomic optimization of compounds **1**-**3**, the kinetic energy cutoff for wavefunctions (ecutwfc) and charge density (ecutrho) were set to 30 and 270 Ry, respectively. The *k*-point was set to 2 × 1 × 1. The convergence threshold on total energy (etot_conv_thr) and force (forc_conv_thr) were 1 × 10^{-4} Ry and 1 × 10^{-3} Ry $Bohr^{-1}$, respectively. After the atomic optimization of the crystal structure, a single-point SCF calculation was carried out. The ecutwfc and ecutrho were set to 64 and 576 Ry, respectively. The *k*-point was set to 3 × 3 × 3. The etot_conv_thr and forc_conv_thr were 3 × 10^{-5} Ry and 3 × 10^{-4} Ry $Bohr^{-1}$, respectively. The resultant energy value was used to the evaluation of the $\Delta\bar{E}_{\mathrm{cry}}$. For the calculation of E_i, the dianthracene (D) and the anthracene pair (AA) were cropped out from the crystal optimized using QE and isolated by the cubic unit cell with the edge of 20 Å.

Table S1. Values (in kJ/mol) of $\bar{E}_{\mathrm{latt}}$ for the anthracene pair ($\bar{E}_{\mathrm{latt}}(\mathrm{AA})$) and the dianthracene ($\bar{E}_{\mathrm{latt}}(\mathrm{D})$), and the energy difference ($\Delta\bar{E}_{\mathrm{latt}}$) of the compounds examined.

	$\bar{E}_{\mathrm{latt}}(\mathbf{AA})$	$\bar{E}_{\mathrm{latt}}(\mathbf{D})$	$\Delta\bar{E}_{\mathrm{latt}}$
Compound 1	−172.3	−138.2	34.1
Compound 2	−168.5	−151.9	16.7
Compound 3	−173.5	−140.2	33.3

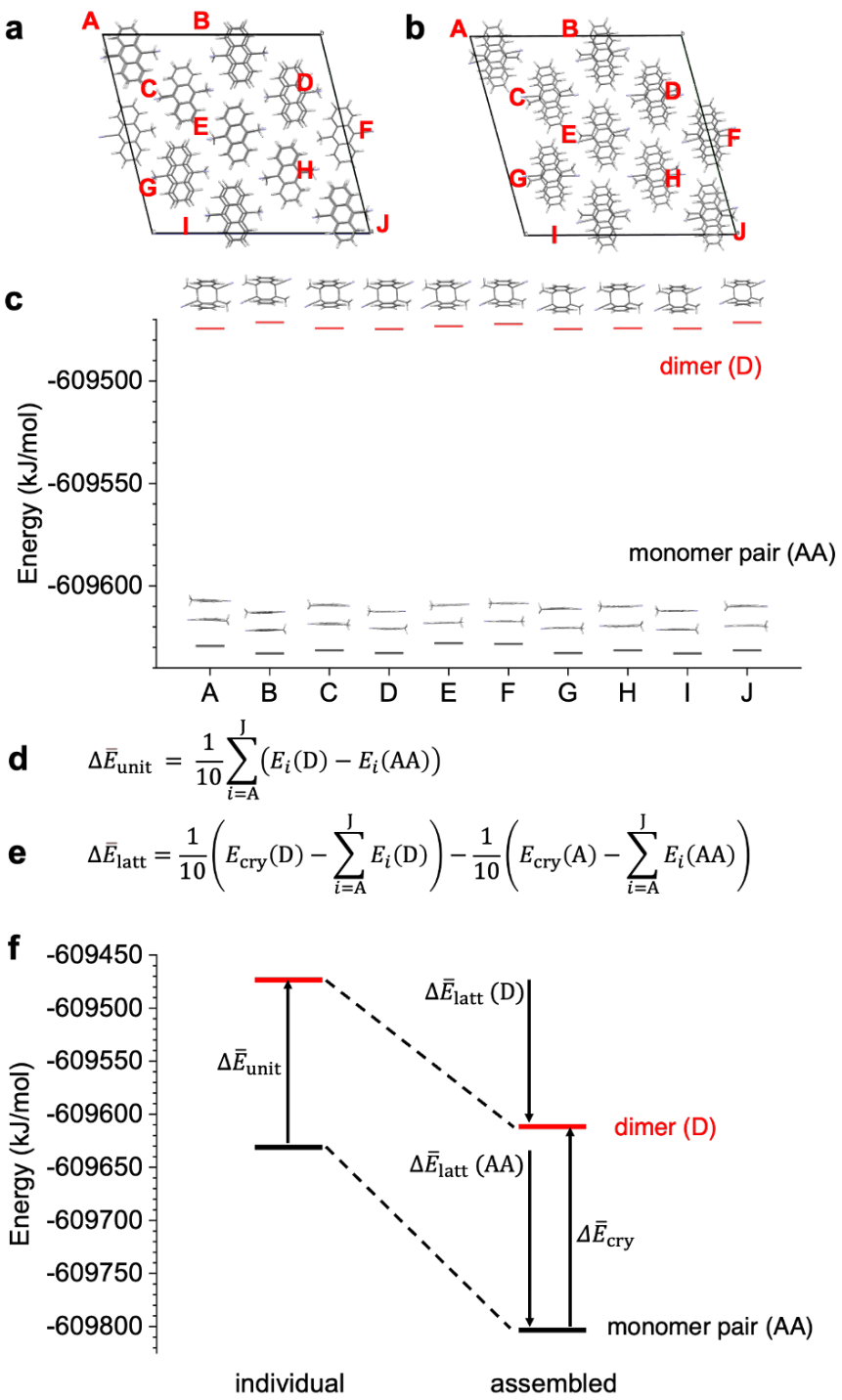

Figure S12. Detailed calculation procedure of $\Delta\bar{E}_{\mathrm{unit}}$ and $\Delta\bar{E}_{\mathrm{latt}}$ for compound **1**. The unit cell of compound **1** for (a) anthracene and (b) dianthracene. Respective cycloaddition units are labeled alphabetically. (c) Energies of all the isolated anthracene pairs cropped out from the crystal structure optimized using QE. (d-e) Equations to calculate $\Delta\bar{E}_{\mathrm{unit}}$ and $\Delta\bar{E}_{\mathrm{latt}}$ for Compound **1** based on the Eq. (1−3). (f) Energy diagram of the relationship among $\Delta\bar{E}_{\mathrm{cry}}$, $\Delta\bar{E}_{\mathrm{unit}}$, and $\Delta\bar{E}_{\mathrm{latt}}$.

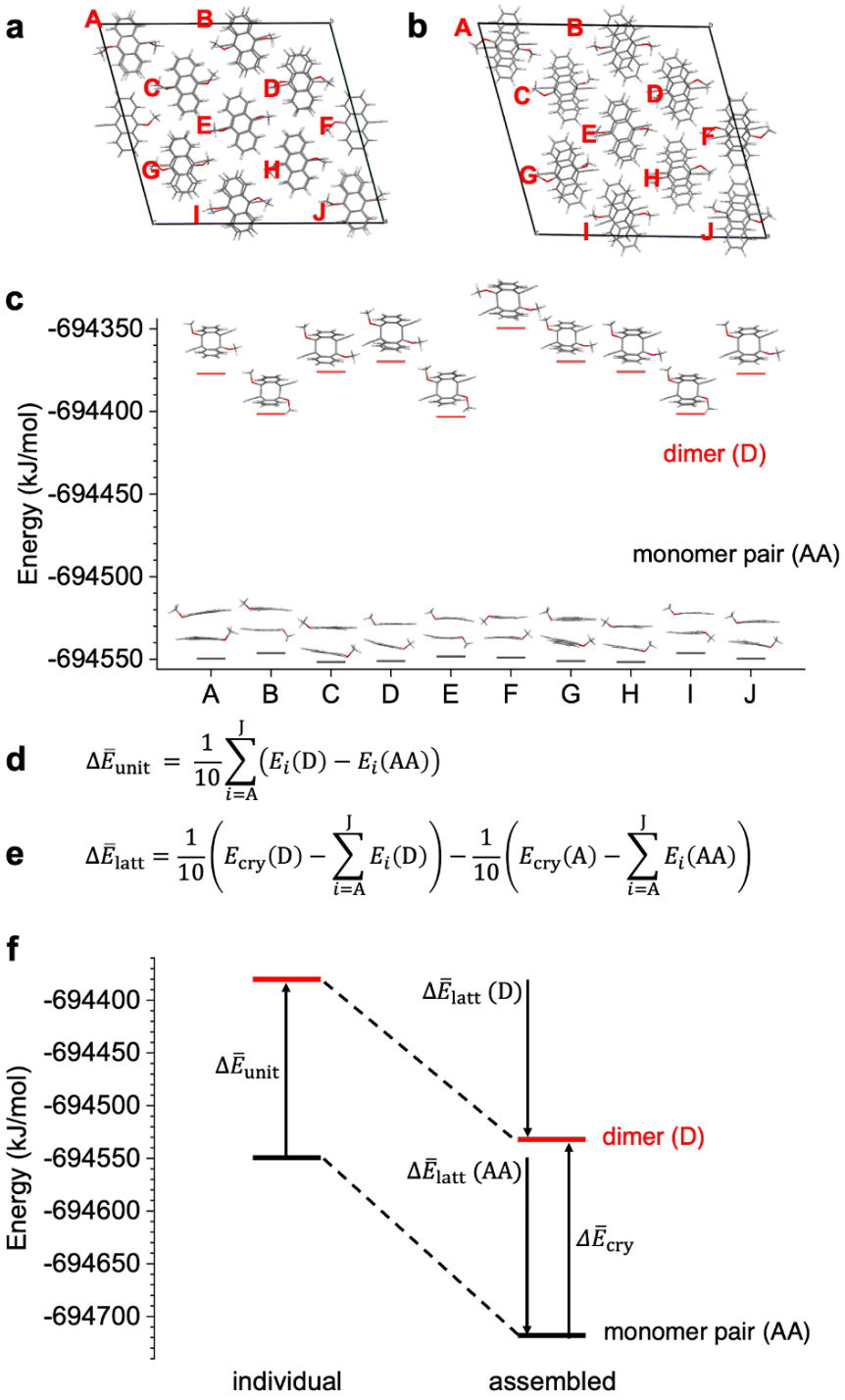

Figure S13. Detailed calculation procedure of $\Delta\bar{E}_{\mathrm{unit}}$ and $\Delta\bar{E}_{\mathrm{latt}}$ for compound **2**. The unit cell of compound **2** for (a) anthracene and (b) dianthracene. Respective cycloaddition units are labeled alphabetically. (c) Energies of all the isolated anthracene pairs cropped out from the crystal structure optimized using QE. (d-e) Equations to calculate $\Delta\bar{E}_{\mathrm{unit}}$ and $\Delta\bar{E}_{\mathrm{latt}}$ for Compound **2** based on the Eq. (1−3). (f) Energy diagram of the relationship among $\Delta\bar{E}_{\mathrm{cry}}$, $\Delta\bar{E}_{\mathrm{unit}}$, and $\Delta\bar{E}_{\mathrm{latt}}$.

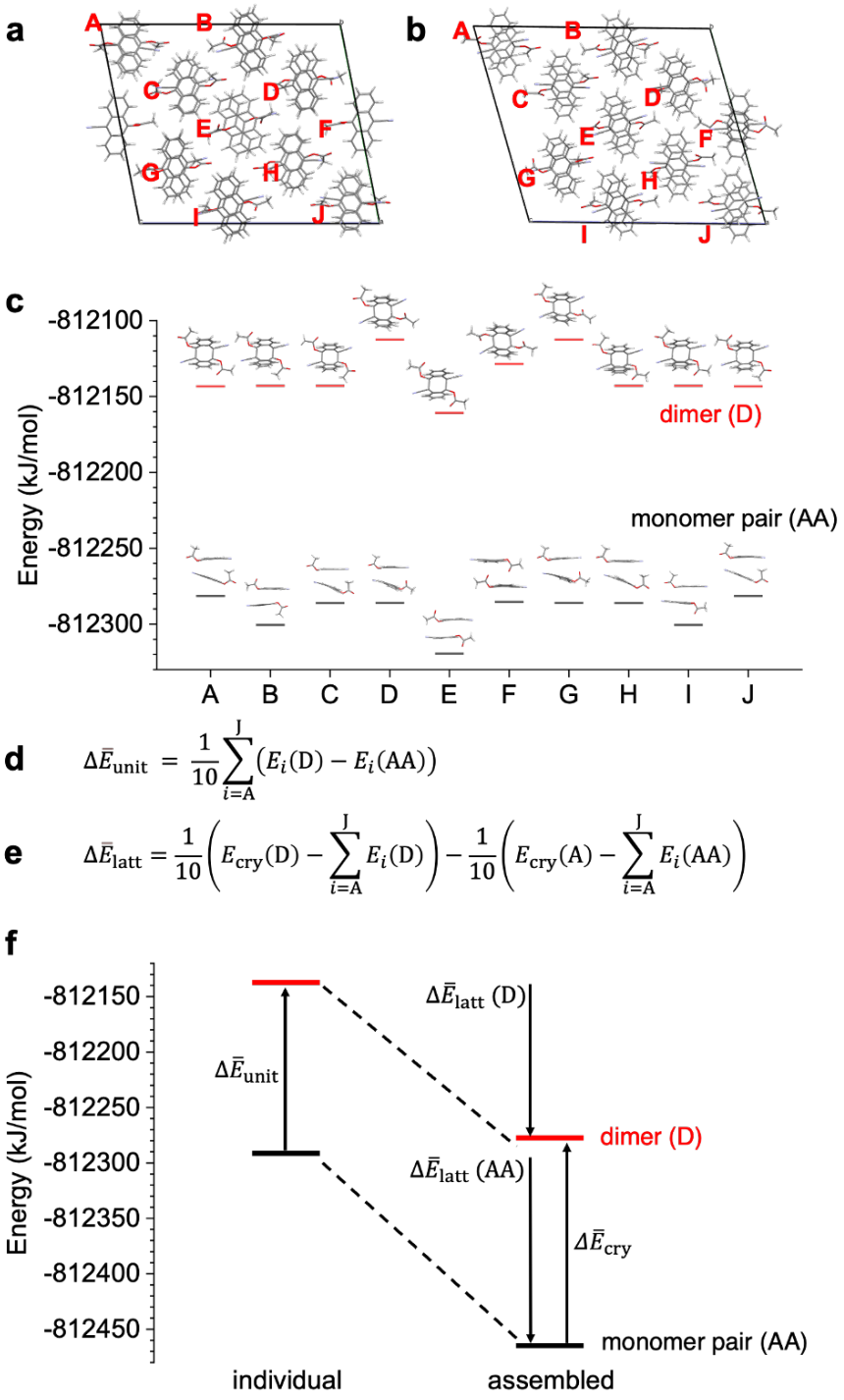

Figure S14. Detailed calculation procedure of $\Delta\bar{E}_{\mathrm{unit}}$ and $\Delta\bar{E}_{\mathrm{latt}}$ for compound **3**. The unit cell of compound **3** for (a) anthracene and (b) dianthracene. Respective cycloaddition units are labeled alphabetically. (c) Energies of all the isolated anthracene pairs cropped out from the crystal structure optimized using QE. (d-e) Equations to calculate $\Delta\bar{E}_{\mathrm{unit}}$ and $\Delta\bar{E}_{\mathrm{latt}}$ for Compound **3** based on the Eq. (1−3). (f) Energy diagram of the relationship among $\Delta\bar{E}_{\mathrm{cry}}$, $\Delta\bar{E}_{\mathrm{unit}}$, and $\Delta\bar{E}_{\mathrm{latt}}$.

References

(1) Chakraborty, S.; Nguyen, H. P. Q.; Usuba, J.; Choi, J. Y.; Sun, Z.; Raju, C.; Sigelmann, G.; Qiu, Q.; Cho, S.; Tenney, S. M.; Shulenberger, K. E; Schmidt-Rohr, K.; Park, J.; Han, G. G. D.. Self-activated energy release cascade from anthracene-based solid-state molecular solar thermal energy storage systems. *Chem* **2024**, *10*, 1-14.

(2) Fung, B. M.; Khitrin, A. K.; Ermolaev, K. An Improved Broadband Decoupling Sequence for Liquid Crystals and Solids. *J. Magn. Reson.* **2000**, *142* (1), 97-101.

(3) Dixon, W. T. Spinning‐sideband‐free and spinning‐sideband‐only NMR spectra in spinning samples. *J. Chem. Phys.* **1982**, *77* (4), 1800-1809.

(4) Thurber, K. R.; Tycko, R. Measurement of sample temperatures under magic-angle spinning from the chemical shift and spin-lattice relaxation rate of 79Br in KBr powder. *J. Magn. Reson.* **2009**, *196* (1), 84-87.

(5) Perdew, J. P.; Burke, K.; Ernzerhof, M. Generalized Gradient Approximation Made Simple. *Phys. Rev. Lett.* **1996**, *77* (18), 3865-3868.

(6) Grimme, S.; Ehrlich, S.; Goerigk, L. Effect of the damping function in dispersion corrected density functional theory. *J. Comput. Chem.* **2011**, *32* (7), 1456-1465.